

# Imaging three-dimensional anisotropic scatterers in multilayered medium by multiple signal classification method with enhanced resolution

Rencheng Song,\* Rui Chen, and Xudong Chen

*Department of Electrical and Computer Engineering, National University of Singapore, 117576 Singapore*

*\*Corresponding author: elesongr@nus.edu.sg*

Received April 30, 2012; accepted July 17, 2012;  
posted July 27, 2012 (Doc. ID 167537); published August 17, 2012

This paper investigates the resolution and robustness of the multiple signal classification (MUSIC) method to locate small three-dimensional (3D) anisotropic scatterers near the medium interface in a multilayered background. An enhanced MUSIC algorithm developed for free-space background is extended to solve such a problem. Because its indicator is built in a stable signal subspace, which is continuous across the medium interface, better stability and higher resolution against noise are observed for the proposed method compared to the known standard MUSIC method. Numerical simulations with various medium interfaces and noise levels are conducted to verify the performance of the introduced MUSIC method. © 2012 Optical Society of America

OCIS codes: 100.3190, 100.6950, 290.3200, 350.4010.

## 1. INTRODUCTION

Inverse scattering methods [1–8] are widely used in optical imaging systems such as Optical Diffraction Tomography (ODT). A sample is illuminated by lights from various directions and scattered fields are measured to retrieve the scatterer's characteristic. This technique is promising in research of medical imaging for detection of tumors in soft tissue [9] as well as in the semiconductor industry for defect inspection [10]. In this paper, we concentrate on an optical imaging method for samples buried in a layered background medium. For extended scatterers, this issue has been studied in [8], where a fast and efficient three-dimensional (3D) semi-quantitative imaging method was introduced. Differently, we consider imaging methods for small 3D scatterers here. The multiple signal classification (MUSIC) method [6,7,11–17] is the target solution, which is a type of qualitative, noniterative, and deterministic method to locate small scatterers. An indicator function (also known as pseudospectrum function), which peaks at the locations of scatterers, is built in the MUSIC method based on the analysis of multistatic response (MSR) matrix [13,17]. So the MUSIC method is also a kind of sampling method. We indicate that many other noniterative imaging methods of small scatterers such as the decomposition of the time reversal operator (DORT) [18] or its related method [19] already exist and we do not plan to give a full review here. Compared to other methods, the MUSIC method is suitable to locate close scatterers at a fixed frequency with super-resolution [20].

Most known MUSIC methods are introduced with homogeneous background medium where Green's function can be obtained analytically. Otherwise, numerical calculation of Green's function is necessary. In [15], the finite element method was applied where the known background obstacles were

of finite size. Although the Green's function in a multilayered infinite medium [21] is semianalytical (in the form of Sommerfeld integrals), numerical integration is still needed. There are already some known MUSIC methods [11–13] for a layered medium. In [11] and [12], two-dimensional (2D) cases were studied in half space and a three-layer background medium, respectively. In [13], 3D scatterers in half space were detected. In all these papers, the standard time reversal MUSIC method was used and all small scatterers were isotropic.

The main interest of this paper is to locate 3D anisotropic small scatterers in a multilayered medium. Different from [13], we focus our point on locating scatterers near the medium interface, which is difficult to solve by the MUSIC method because of strong influence by the medium interface. In such a case, the stability and imaging resolution of the MUSIC method against noise are mainly concerned. We find the performance of the standard MUSIC method depends on the choice of the orientation of test diople. Furthermore, the indicator of standard MUSIC method is discontinuous across the interface, which makes it difficult to judge the location of scatterers near interface. To increase the stability and resolution of the imaging algorithm, we apply an enhanced MUSIC method to locate scatterers in a multilayered medium. Its indicator is built with a stable signal subspace and the optimal test direction is chosen at each test node. Therefore, it is more stable against noise. Moreover, we prove that the new indicator function is continuous across interfaces. Therefore, our method has better performance than the standard one to locate 3D anisotropic scatterers that are near medium interface. Numerical simulations confirm the above advantages of the enhanced MUSIC method.

The structure of this paper is as follows. In Section 2, the forward model of electromagnetic scattering in a layered

medium is built based on the Foldy–Lax equation. Then the inverse scattering model as well as the standard and enhanced MUSIC methods are introduced in Section 3. Numerical examples are shown in Section 4. Finally, we make conclusions in Section 5.

## 2. FORWARD SCATTERING MODEL

Let vectors and matrices be denoted by letters with single and double bars, respectively. The background consists of several layers of media, each being homogeneous. Consider  $M$  3D spherical anisotropic scatterers at  $\{\bar{s}_j\}_{j=1}^M$ , which are illuminated by electromagnetic waves from  $N$  transmitters located at  $\{\bar{r}_j\}_{j=1}^N$ . Suppose the receivers are coincident with transmitters. Each transceiver consists of three antennas, oriented in the  $x$ ,  $y$ , and  $z$  directions, respectively. The permittivity tensor of the  $m$ th scatterers is given as

$$\bar{\bar{\epsilon}}_m = \begin{bmatrix} \epsilon_m^{xx} & \epsilon_m^{xy} & \epsilon_m^{xz} \\ \epsilon_m^{yx} & \epsilon_m^{yy} & \epsilon_m^{yz} \\ \epsilon_m^{zx} & \epsilon_m^{zy} & \epsilon_m^{zz} \end{bmatrix} = \bar{\bar{\Xi}}_{E,m}^{-1} \begin{bmatrix} \epsilon_m^{(1)} & 0 & 0 \\ 0 & \epsilon_m^{(2)} & 0 \\ 0 & 0 & \epsilon_m^{(3)} \end{bmatrix} \bar{\bar{\Xi}}_{E,m}, \quad (1)$$

where  $\bar{\bar{\Xi}}_{E,m}$  is the rotation transforming matrix composed by Euler angles [17], and  $\epsilon_m^{(j)}$  ( $j = 1, 2, 3$ ) is the permittivity element aligned to the  $j$ th electric principal axis of the  $m$ th scatterer. Suppose all materials are nonmagnetic, i.e.,  $\mu = \mu_0$ .

### A. The MSR Matrix

Suppose  $\bar{E}_t^{\text{in}}(\bar{s}_j)$  is the total electric field incident upon the  $j$ th scatterer at  $\bar{s}_j$  and  $\bar{E}^{\text{sca}}(\bar{r}_l)$  is the scattered field measured by the antenna at  $\bar{r}_l$ . Following a similar analysis as in [17], the Foldy–Lax equation of electromagnetic scattering for small scatterers in a layered medium can be obtained as

$$\bar{E}_t^{\text{in}}(\bar{s}_j) = \bar{E}_0^{\text{in}}(\bar{s}_j) + \sum_{m=1, m \neq j}^M \{i\omega\mu_0 \bar{G}(\bar{s}_j, \bar{s}_m) \cdot \bar{\bar{\xi}}_m(\epsilon_b(\bar{s}_m)) \cdot \bar{E}_t^{\text{in}}(\bar{s}_m)\}, \quad j = 1, 2, \dots, M, \quad (2)$$

$$\bar{E}^{\text{sca}}(\bar{r}_l) = \sum_{m=1}^M \{i\omega\mu_0 \bar{G}(\bar{r}_l, \bar{s}_m) \cdot \bar{\bar{\xi}}_m(\epsilon_b(\bar{s}_m)) \cdot \bar{E}_t^{\text{in}}(\bar{s}_m)\}, \quad l = 1, 2, \dots, N, \quad (3)$$

where  $\epsilon_b(\bar{s}_m)$  is the background permittivity at  $\bar{s}_m$ ,  $\bar{E}_0^{\text{in}}(\bar{s}_j)$  is the background incident wave at  $\bar{s}_j$ ,  $\bar{G}(\bar{s}_j, \bar{s}_m)$  is the dyadic Green's function in a layered medium [21], and

$$\bar{\bar{\xi}}_m(\epsilon_b(\bar{s}_m)) = -i4\pi k_b(\bar{s}_m) a_m^3 \sqrt{\frac{\epsilon_b(\bar{s}_m)}{\mu_0}} \bar{\bar{\Xi}}_{E,m}^{-1} \cdot \text{diag} \left[ \frac{\epsilon_m^{(1)} - \epsilon_b(\bar{s}_m)}{\epsilon_m^{(1)} + 2\epsilon_b(\bar{s}_m)}, \frac{\epsilon_m^{(2)} - \epsilon_b(\bar{s}_m)}{\epsilon_m^{(2)} + 2\epsilon_b(\bar{s}_m)}, \frac{\epsilon_m^{(3)} - \epsilon_b(\bar{s}_m)}{\epsilon_m^{(3)} + 2\epsilon_b(\bar{s}_m)} \right] \cdot \bar{\bar{\Xi}}_{E,m} \quad (4)$$

is the polarization parameter with  $k_b(\bar{s}_m)$  the wavenumber at  $\bar{s}_m$  and  $a_m$  the radius of the  $m$ th scatterer. We should indicate

that  $\bar{\bar{\xi}}_m$  in Eq. (4) is consistent with the result in [13] obtained by asymptotic analysis.

Based on Eqs. (2) and (3), the MSR matrix [14,17] is obtained as

$$\bar{\bar{A}} = \bar{\bar{R}} \cdot \bar{\bar{\Lambda}} \cdot (\bar{\bar{I}} - \bar{\bar{\Phi}} \cdot \bar{\bar{\Lambda}})^{-1} \cdot \bar{\bar{R}}^T, \quad (5)$$

where  $\bar{\bar{R}}(i, j) = i\omega\mu_0 \bar{G}(\bar{r}_i, \bar{s}_j)$ , the superscript  $T$  denotes transpose,  $\bar{\bar{\Phi}}(j, k)$  is null for  $j = k$  and otherwise  $i\omega\mu_0 \bar{G}(\bar{s}_j, \bar{s}_k)$ ,  $\bar{\bar{I}}$  is the identity matrix, and  $\bar{\bar{\Lambda}} = \text{diag}(\bar{\bar{\xi}}_1(\epsilon_b(\bar{s}_1)), \bar{\bar{\xi}}_2(\epsilon_b(\bar{s}_2)), \dots, \bar{\bar{\xi}}_M(\epsilon_b(\bar{s}_M)))$ .

## 3. INVERSE SCATTERING PROBLEM AND MUSIC METHODS

The inverse scattering problem is to determine locations of small scatterers from the measured scattered fields stored in  $3N \times 3N$  matrix  $\bar{\bar{A}}$ , which is called the MSR matrix. The element of  $\bar{\bar{A}}$  in the  $i$ th row and  $j$ th column denotes the measured scattered field at the  $i$ th antenna for a unitary excitation at the  $j$ th antenna. Define  $3N \times 3$  test matrix  $\bar{\bar{Q}}(\bar{s}) = [\bar{G}^T(\bar{r}_1, \bar{s}), \bar{G}^T(\bar{r}_2, \bar{s}), \dots, \bar{G}^T(\bar{r}_N, \bar{s})]^T$ , where  $\bar{G}(\bar{r}_j, \bar{s})$  is the dyadic Green's function in a layered medium [21] observed at  $\bar{r}_j$  due to source at  $\bar{s}$ .

Suppose the singular value decomposition (SVD) of the MSR matrix is  $\bar{\bar{A}} = \bar{\bar{U}} \bar{\bar{\Sigma}} \bar{\bar{V}}^H$ , where  $H$  indicates the conjugate transpose. In a component form, there is  $\bar{\bar{A}} \cdot \bar{v}_p = \sigma_p \bar{u}_p$ ,  $p = 1, 2, \dots, 3N$ . Define two subspaces

$$U_S = \text{span}\{\bar{u}_p, \sigma_p > 0\} = \text{span}\{\bar{u}_1, \bar{u}_2, \dots, \bar{u}_K\},$$

$$U_N = \text{span}\{\bar{u}_p, \sigma_p = 0\} = \text{span}\{\bar{u}_{K+1}, \bar{u}_{K+2}, \dots, \bar{u}_{3N}\},$$

which are called signal and noise spaces, respectively. The integer  $K$  denotes the rank of the MSR matrix  $\bar{\bar{A}}$ .

### A. Two Kinds of Indicators in MUSIC Methods

The MUSIC method is based on the fact that if the size of the MSR matrix  $\bar{\bar{A}}$  is sufficiently large, there is

$$\bar{\bar{Q}}(\bar{s}) \cdot \bar{a} \in U_S \quad \text{if and only if } \bar{s} \in \{\bar{s}_1, \bar{s}_2, \dots, \bar{s}_M\}$$

for arbitrary nonzero 3D vector  $\bar{a}$ . For detailed proof, please refer to [14,22].

Therefore, the indicator function of standard MUSIC [13] is defined as

$$W_1(\bar{a}, \bar{s}) = \frac{1}{\sum_{i=K+1}^{3N} |\bar{u}_i^H \cdot \bar{\bar{Q}}(\bar{s}) \cdot \bar{a}|^2}, \quad (6)$$

where  $\bar{a}$  is an arbitrarily given test direction. The indicator  $W_1(\bar{a}, \bar{s})$  peaks at any of the scatterer locations  $\{\bar{s}_j\}_{j=1}^M$ .

$W_1(\bar{a}, \bar{s})$  in Eq. (6) is defined with noise space  $U_N$ . Alternatively, we can also find its equivalent form with signal space  $U_S$ . Let  $\bar{v}(\bar{a}, \bar{s}) = \bar{\bar{Q}}(\bar{s}) \cdot \bar{a}$ . Then  $\bar{v}(\bar{a}, \bar{s})$  has zero angle with  $U_S$  if and only if  $\bar{s} \in \{\bar{s}_j\}_{j=1}^M$ . For a given  $\bar{v}(\bar{a}, \bar{s})$ , suppose its angle with  $U_S$  is  $\theta(\bar{a}, \bar{s})$ . Then  $\theta(\bar{a}, \bar{s})$  satisfies that

$$\cos(\theta(\bar{a}, \bar{s})) = \frac{|\bar{q}(\bar{a}, \bar{s})|}{|\bar{v}(\bar{a}, \bar{s})|}, \quad (7)$$

where  $|\cdot|$  denotes the vector length and  $\bar{q}(\bar{a}, \bar{s}) = [\bar{u}_1, \bar{u}_2, \dots, \bar{u}_K]^H \cdot \bar{v}(\bar{a}, \bar{s})$  is the orthogonal projection of  $\bar{v}(\bar{a}, \bar{s})$  into  $U_S$ . With the help of the definition in Eq. (7), we can rewrite  $W_1(\bar{a}, \bar{s})$  with signal space  $U_S$  as

$$W_1(\bar{a}, \bar{s}) = \frac{1}{(1 - \cos^2(\theta))|\bar{v}(\bar{a}, \bar{s})|}. \quad (8)$$

In comparison, the indicator of the enhanced MUSIC method is derived with three changes done on  $W_1$  in Eq. (8). **First, at each test node  $\bar{s}$ , the fixed  $\bar{a}$  in  $W_1$  is changed to the optimal one  $\bar{a}_{\text{opt}}(\bar{s})$  [14], which makes  $\bar{v}(\bar{a}, \bar{s})$  have the smallest angle  $\theta_{\min}(\bar{s})$  with  $U_S$ . Second, the whole signal space  $U_S$  is changed to a more stable subspace  $U_L = \text{span}\{\bar{u}_1, \bar{u}_2, \dots, \bar{u}_L\}$ , where  $L < K$ . Third, a normalization has been done on  $\bar{v}(\bar{a}, \bar{s})$ . Therefore, the indicator function of the enhanced MUSIC method is defined as**

$$W_2(\bar{a}_{\text{opt}}(\bar{s}), \bar{s}) = \frac{1}{1 - \cos^2(\theta_{\min}(\bar{s}))}. \quad (9)$$

At each test node  $\bar{s}$ ,  $\theta_{\min}(\bar{s})$  can be determined by searching  $\bar{a}_{\text{opt}}(\bar{s})$  ( $|\bar{a}_{\text{opt}}(\bar{s})| = 1$ ) from

$$\bar{a}_{\text{opt}}(\bar{s}) = \arg \max_{\bar{a}} \frac{\sum_{i=1}^L |\bar{u}_i^H \cdot \bar{Q}(\bar{s}) \cdot \bar{a}|^2}{|\bar{Q}(\bar{s}) \cdot \bar{a}|^2}, \quad (10)$$

which needs to solve an eigendecomposition of a  $3 \times 3$  matrix [14]. On the other hand, the dimension  $L$  of stable subspace  $U_L$  in Eq. (9) needs to be determined based on the solvability of  $\bar{a}_{\text{opt}}$ . Here we list the rule to determine  $L$  without proof. For detail, please refer to [14]. To locate the  $j$ th scatterer,  $L$  should be at least  $P_j + 1$ , where  $P_j = \sum_{i=1, i \neq j}^M \text{rank}(\bar{\xi}_i)$ . Then the minimal  $L$  to locate all of the scatterers is  $L = \max_j \{P_j\} + 1$ , which is smaller than  $K$ .

## B. Comparison of the Two MUSIC Methods in Layered Medium

Two issues of MUSIC methods in a layered medium, the stability against noise and the continuity of indicators at medium interface, are discussed here. They are closely related to the imaging resolution of MUSIC methods.

Firstly, the MUSIC method is said to be stable if its results do not change too much with various test directions and noise levels. We denote the noise-contaminated MSR matrix as  $\bar{A}'$ . Suppose its SVD is  $\bar{A}' \cdot \bar{v}_p = \sigma_p' \bar{u}_p'$ ,  $p = 1, 2, \dots, 3N$ . All singular values of  $\bar{A}'$  are positive ( $\sigma_p' > 0$  for  $p = 1, 2, \dots, 3N$ ) due to the existence of noise. Therefore, it is difficult to separate the signal and noise spaces directly as the noiseless case. If the signal and noise spaces of  $\bar{A}'$  are formally represented as

$$U'_S = \text{span}\{\bar{u}'_1, \bar{u}'_2, \dots, \bar{u}'_K\}, \\ U'_N = \text{span}\{\bar{u}'_{K+1}, \bar{u}'_{K+2}, \dots, \bar{u}'_{3N}\},$$

then  $U'_N$  must overlap with  $U_S$  due to noise. As seen in Eq. (8),  $W_1(\bar{a}, \bar{s})$  is constructed with the whole signal space  $U_S$ . For a given test direction  $\bar{a}$ , if  $\bar{v}(\bar{a}, \bar{s}_j)$  falls into the overlapping region  $U_S \cap U'_N$ , the scatterer  $\bar{s}_j$  may be lost (depending on the overlapping level) by the indicator  $W_1(\bar{a}, \bar{s})$ . Although the test direction  $\bar{a}$  obviously affects the imaging results, there is no rule given in the standard MUSIC method for choosing proper

$\bar{a}$  in a layered medium, especially when scatterers are near medium interface.

In comparison,  $W_2(\bar{a}_{\text{opt}}(\bar{s}), \bar{s})$  is defined in a subspace  $U_L$  instead of  $U_S$ , as shown in Eq. (9). Since  $U_S$  overlaps with  $U'_N$  mostly at those singular vectors corresponding to small singular values, the overlapping effect is suppressed in  $U_L$  compared with  $U_S$ . This is because the former is a subspace of the latter by taking the first  $L$  leading components. Furthermore, optimal test direction is chosen at each node with very cheap computational cost. For the two reasons,  $W_2(\bar{a}_{\text{opt}}(\bar{s}), \bar{s})$  is said to be more stable against noise than  $W_1(\bar{a}, \bar{s})$ .

Secondly,  $W_1(\bar{a}, \bar{s})$  is discontinuous across the medium interface if the test direction  $\bar{a}$  is not parallel to this interface plane. Suppose one medium interface is located at plane  $z = z_0$ . For a source at  $\bar{s}$ , the dyadic Green's function in the layered medium has form  $\bar{G}(\bar{r}, \bar{s}) = (\bar{G}_x^T, \bar{G}_y^T, \bar{G}_z^T)^T(\bar{r}, \bar{s})$ , where  $\bar{G}_x$ ,  $\bar{G}_y$ , and  $\bar{G}_z$  are the first, second, and third rows of  $\bar{G}(\bar{r}, \bar{s})$ , respectively. The boundary condition requires that the tangential components of electric field and the normal component of electric displacement field are continuous at interface, namely

$$\bar{G}_x(\bar{r}_+, \bar{s}) = \bar{G}_x(\bar{r}_-, \bar{s}), \bar{G}_y(\bar{r}_+, \bar{s}) = \bar{G}_y(\bar{r}_-, \bar{s}), \\ \epsilon_r(\bar{r}_+) \bar{G}_z(\bar{r}_+, \bar{s}) = \epsilon_r(\bar{r}_-) \bar{G}_z(\bar{r}_-, \bar{s}), \quad (11)$$

where  $\bar{r}$  is an arbitrary position on interface,  $\bar{r}_{+,-}$  represents the position approaching  $\bar{r}$  from up and down layers, respectively, and  $\epsilon_r(\bar{r}_{+,-})$  are the corresponding relative permittivities in the two neighboring layers.

From the reciprocity of dyadic Green's function,  $\bar{Q}(\bar{s})$  in Eq. (6) can be rewritten as

$$\bar{Q}(\bar{s}) = [\bar{Q}_x, \bar{Q}_y, \bar{Q}_z] = [\bar{G}^T(\bar{r}_1, \bar{s}), \bar{G}^T(\bar{r}_2, \bar{s}), \dots, \bar{G}^T(\bar{r}_N, \bar{s})]^T, \quad (12) \\ = [\bar{G}(\bar{s}, \bar{r}_1), \bar{G}(\bar{s}, \bar{r}_2), \dots, \bar{G}(\bar{s}, \bar{r}_N)]^T. \quad (13)$$

From Eq. (11), when the test node  $\bar{s}$  is on the interface, there is

$$\bar{Q}_x(\bar{s}_+) = \bar{Q}_x(\bar{s}_-), \bar{Q}_y(\bar{s}_+) = \bar{Q}_y(\bar{s}_-), \\ \epsilon_r(\bar{s}_+) \bar{Q}_z(\bar{s}_+) = \epsilon_r(\bar{s}_-) \bar{Q}_z(\bar{s}_-). \quad (14)$$

$\bar{Q}_z(\bar{s})$  jumps at the medium interface plane, as seen from Eq. (14). Therefore, from the definition of indicator in Eq. (6),  $W_1(\bar{a}, \bar{s})$  is discontinuous across the medium interface if  $\bar{a}$  is not parallel to interface plane, e.g.,  $\bar{a} = (0, 0, 1)^T$ . Particularly, the discontinuity will be more obvious if the permittivity contrast of the two sides increases. Because the MUSIC method locates scatterers by the contrast of indicator values at different test nodes, the discontinuity of  $W_1(\bar{a}, \bar{s})$  makes it difficult to judge the locations of scatterers near medium interface.

In comparison,  $W_2(\bar{a}_{\text{opt}}(\bar{s}), \bar{s})$  is continuous at interface nodes. This is due to use of the optimal test direction at each node in  $W_2(\bar{a}_{\text{opt}}(\bar{s}), \bar{s})$ . For arbitrary test node  $\bar{s}$  on interface,  $\bar{Q}(\bar{s}_+)$  and  $\bar{Q}(\bar{s}_-)$  are connected by Eq. (14). This implies  $\theta_{\min}(\bar{s}_+)$  and  $\theta_{\min}(\bar{s}_-)$  must be the same. If the optimal test direction at  $\bar{s}_+$  is  $\bar{a}_{\text{opt}}(\bar{s}_+) = [a_1, a_2, a_3]^T$ , then the optimal test direction  $\bar{a}_{\text{opt}}(\bar{s}_-)$  at  $\bar{s}_-$  should be  $\bar{a}_{\text{opt}}(\bar{s}_-) = \bar{b}/|\bar{b}|$  with  $\bar{b} = [a_1, a_2, \epsilon(\bar{s}_-)/\epsilon(\bar{s}_+) \cdot a_3]^T$ . So  $W_2(\bar{a}_{\text{opt}}(\bar{s}), \bar{s})$  is continuous across the medium interface. This is the second advantage

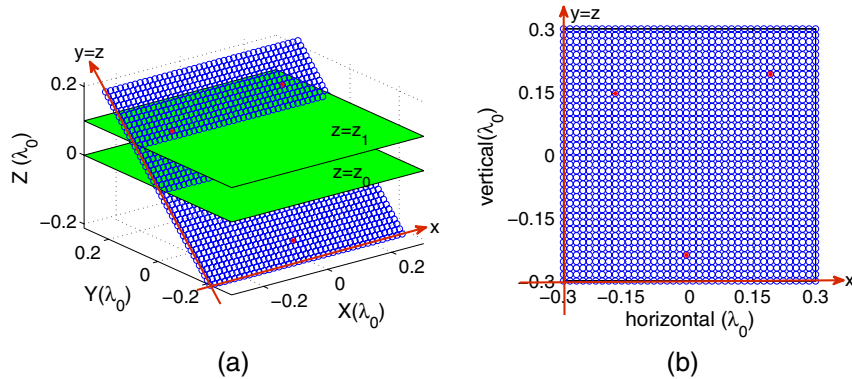


Fig. 1. (Color online) Problem sketch of inverse scattering: (a) the 3D view of the problem where the green plane indicates the medium interface; (b) the 2D view of scatterer locations on  $y = z$  plane, where the square domain of interest is denoted by blue points and the red points are the locations of scatterers.

of enhanced MUSIC over the standard one in a layered medium.

Finally, we also indicate two major differences of our paper compared to [14]. First, the concerned background medium here is layered and the aforementioned discontinuity of the pseudospectrum at interface needs to be analyzed. Second, comparisons between the two MUSIC methods are done here for nondegenerate scatterers, whereas [14] focuses mainly on degenerate scatterers.

### 4. NUMERICAL SIMULATIONS

In this section, some numerical simulations are done to verify the theoretical discussions above. Comparisons are made between the standard and enhanced MUSIC methods. Two main cases are considered, i.e., different medium interface locations and different noise levels. The experimental configuration is introduced first. We consider a three-layer background medium here, as shown in Fig. 1. Suppose the working frequency is 300 MHz. The permittivities from top to bottom layers are  $\epsilon_0$ ,  $5\epsilon_0$ , and  $\epsilon_0$ , respectively, where  $\epsilon_0$

is the permittivity of free space. There are 16 receivers (transmitters are coincident with receivers) locating at the  $z = 10\lambda_0$  plane, where  $\lambda_0$  is the wavelength of the uppermost layer. Transceivers are uniformly distributed in  $x$ -axis and  $y$ -axis. Half of the transceivers are along the  $x$ -axis, while the rest are along the  $y$ -axis, where they are centered at the  $(0, 0, 10\lambda_0)$  and the distance of two neighboring transceivers is  $5\lambda_0$ . The two medium interfaces are located at  $z = z_0\lambda_0$  and  $z = z_1\lambda_0$  ( $z_0 < z_1$ ), respectively. The dyadic Green's function in a layered medium is computed by the method in [21].

Three scatterers are considered with locations  $\bar{s}_1 = (-0.177, 0.103, 0.103)\lambda_0$ ,  $\bar{s}_2 = (0.192, 0.136, 0.136)\lambda_0$ , and  $\bar{s}_3 = (-0.008, -0.169, -0.169)\lambda_0$ . All three of these scatterers have radius  $a = \frac{\lambda_0}{30}$  and their permittivities are  $\bar{\epsilon}_1 = \text{diag}(3\epsilon_0, 3\epsilon_0, 3\epsilon_0)$ ,  $\bar{\epsilon}_2 = \text{diag}(2\epsilon_0, 3\epsilon_0, 3\epsilon_0)$ , and  $\bar{\epsilon}_3 = \text{diag}(2\epsilon_0, 2\epsilon_0, 4\epsilon_0)$ , respectively. Correspondingly, the Euler angles in Eq. (1) are set as  $[\frac{\pi}{3}, \frac{2\pi}{5}, \frac{4\pi}{7}]$ . The domain of interest is chosen as a square domain  $[-0.3, 0.3]\lambda_0 \times [-0.3, 0.3]\lambda_0$  centered at

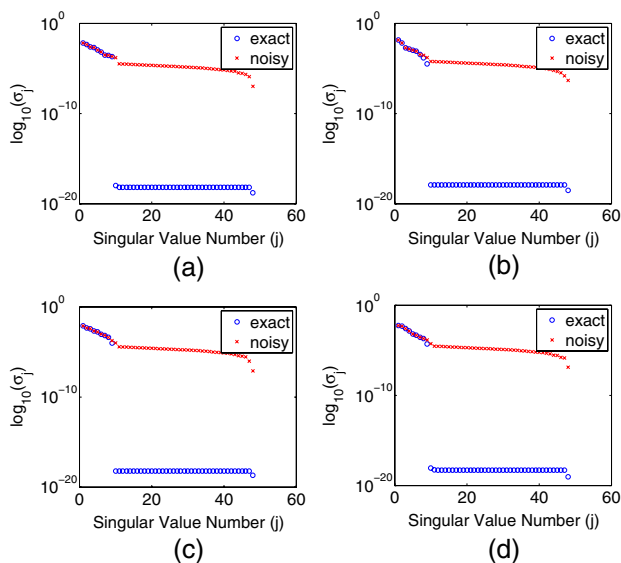


Fig. 2. (Color online) Singular values of MSR matrices with 30 dB white Gaussian noise under different medium interfaces: (a)  $[z_0, z_1] = [0, 0.2]\lambda_0$ , (b)  $[z_0, z_1] = [-0.2, 0.2]\lambda_0$ , (c)  $[z_0, z_1] = [0, 0.05]\lambda_0$ , and (d)  $[z_0, z_1] = [0, 0.12]\lambda_0$ .

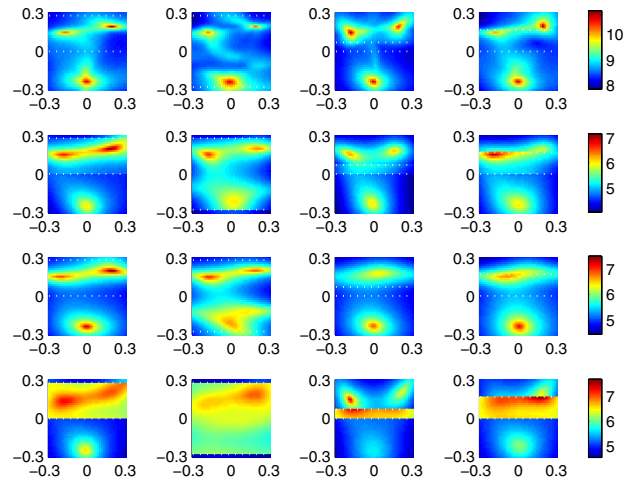


Fig. 3. (Color online) 10-base-logarithm pseudospectrums of MUSIC algorithms with different medium interfaces. The white dotted line represents the interface location. Each column corresponds to results with one given interface configuration: the first column  $[z_0, z_1] = [0, 0.2]\lambda_0$ , the second column  $[z_0, z_1] = [-0.2, 0.2]\lambda_0$ , the third column  $[z_0, z_1] = [0, 0.05]\lambda_0$ , and the fourth column  $[z_0, z_1] = [0, 0.12]\lambda_0$ . Each row corresponds to the results of a method: the first row enhanced MUSIC, the second row standard MUSIC with  $\bar{a}_1 = (1, 1, 1)^T$ , the third row standard MUSIC with  $\bar{a}_2 = (1, 0, 0)^T$ , and the fourth row standard MUSIC with  $\bar{a}_3 = (0, 0, 1)^T$ .

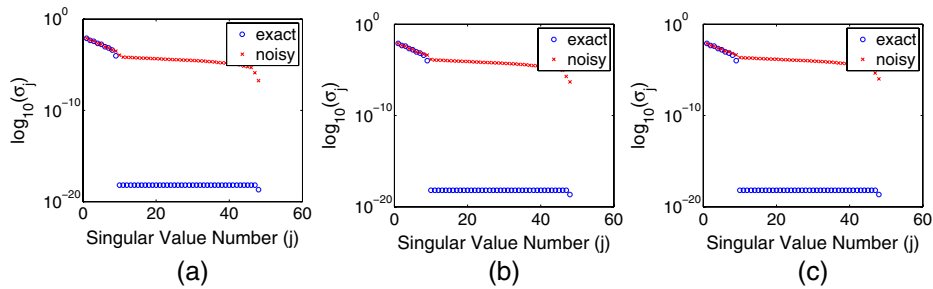


Fig. 4. (Color online) Singular values of MSR matrices with different noise levels where medium interfaces are at  $[z_0, z_1] = [0, 0.05]\lambda_0$ : (a) 25 dB, (b) 20 dB, and (c) 15 dB.

$(0,0,0)$  on the  $y = z$  plane, as shown in Fig. 1, in which the horizontal axis represents the  $x$ -axis and the vertical axis is along line  $y = z$ .

Four groups of interfaces are considered in this paper. They are  $[z_0, z_1] = [0, 0.2]\lambda_0$ ,  $[-0.2, 0.2]\lambda_0$ ,  $[0, 0.05]\lambda_0$ , and  $[0, 0.12]\lambda_0$ , respectively. Three different test directions,  $\bar{a}_1 = (1, 1, 1)^T$ ,  $\bar{a}_2 = (1, 0, 0)^T$ , and  $\bar{a}_3 = (0, 0, 1)^T$  are tested for the standard MUSIC method.  $K = 9$  and  $L = 7$  are used respectively in the two indicators in Eqs. (8) and (9).

In the first case, 30 dB additive Gaussian white noise [14] is added to the MSR matrix obtained under different medium interface locations. From the above problem configuration, it is known that the rank of  $\bar{A}$  without noise is 9. As seen in Fig. 2, we observe that the small singular values raise a lot due to noise and this makes it difficult to distinguish the signal and noise spaces. The indicator values (pseudospectrums) of the two MUSIC methods are shown in Fig. 3. In this figure, each column corresponds to pseudospectrums of the two MUSIC methods with a group of given interface locations. And from top to bottom rows, the results are in sequence the enhanced MUSIC with  $\bar{a}_{opt}$  and the standard MUSIC with  $\bar{a}_j$ ,  $j = 1, 2, 3$ . The white dotted line represents the interface location in the domain of interest.

We observe that the standard MUSIC method fails to locate all the three scatterers in most cases. Its results turn out to depend prominently on test directions. Particularly, the pseudospectrums of standard MUSIC with  $\bar{a}_1$  and  $\bar{a}_3$  are discontinuous at the interfaces and the discontinuity of  $\bar{a}_3$  is much stronger than  $\bar{a}_1$ . This is because they are not parallel to interface planes and  $\bar{a}_3$  has a larger angle with interface compared to  $\bar{a}_1$ . In comparison, the enhanced MUSIC method works well in all four kinds of interface configurations. Obviously, its pseudospectrums are continuous across interfaces. For this example, the performance of the standard MUSIC method depends seriously on the test direction and interface locations. Its results become worse when the test direction is perpendicular to interface plane or scatterers are close to interface. In comparison, the enhanced MUSIC method is stable and has better resolution. These results are consistent with the analysis in Section 3.

In the second case, we compare the two MUSIC methods with higher noises. Different noise levels such as 25, 20, and 15 dB are tested respectively. Only medium interfaces at  $[z_0, z_1] = [0, 0.05]\lambda_0$  are considered here. The results of other three interface configurations shown above are similar and omitted here. Figure 4 shows the singular values of the MSR matrix with and without noise. From this figure, we see that more singular values raise when noise level increases.

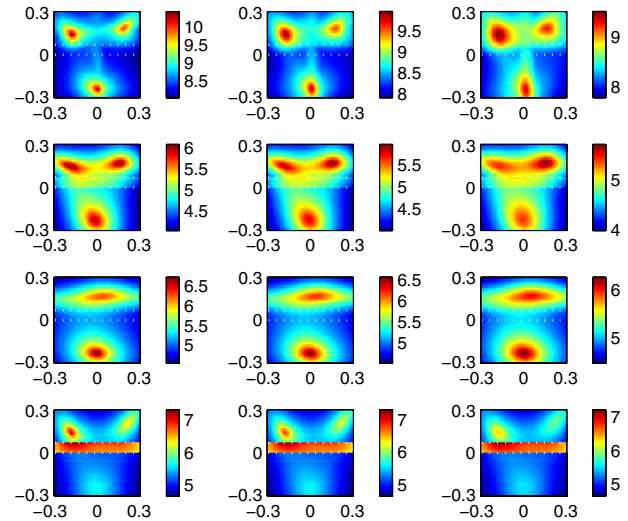


Fig. 5. (Color online) 10-base-logarithm pseudospectrums of MUSIC algorithms with different noise levels where medium interfaces are at  $[z_0, z_1] = [0, 0.05]\lambda_0$ . The white dotted line represents the interface location. Each column corresponds to results with one given noise level: the first column 25 dB, the second column 20 dB, and the third column 15 dB. Each row corresponds to results of a method: the first row enhanced MUSIC, the second row standard MUSIC with  $\bar{a}_1 = (1, 1, 1)^T$ , the third row standard MUSIC with  $\bar{a}_2 = (1, 0, 0)^T$ , and the fourth row standard MUSIC with  $\bar{a}_3 = (0, 0, 1)^T$ .

This means the overlapping region of  $U_S$  and  $U'_N$  are enlarged, which makes the problem more difficult to solve by the MUSIC method. The corresponding pseudospectrums of the two MUSIC methods are shown in Fig. 5. We observe that the results of enhanced MUSIC are still satisfactory for higher noises. In comparison, the results of the standard MUSIC method become worse when noise increases. This example verifies the good stability of the enhanced MUSIC method against noise.

### 5. CONCLUSIONS

In this paper, small 3D anisotropic scatterers have been successfully retrieved by the enhanced MUSIC algorithm in a multilayered medium, which has been numerically verified by different interface configurations and noise levels. Our method builds the indicator that uses the signal subspace and seeks an optimal test direction at each node. Therefore, it has a continuous indicator across the medium interface and it is more stable against noise. These good characteristics make the enhanced MUSIC method a better candidate than the standard

one to locate scatterers near the interface in a layered medium.

We should indicate that the measured data in this paper is full wave, i.e., both the intensity and phase of scattered field are available. In some optical imaging systems, when the working frequency is too high, only intensity data can be obtained because it is difficult to measure phase data at high frequencies. Therefore, an extension of the present method to intensity-only data is our future work.

## ACKNOWLEDGMENTS

This work was supported by the Singapore Ministry of Education under grant R263000575112.

## REFERENCES

1. P. van den Berg and A. Abubakar, "Optical microscopy imaging using the contrast source inversion method," *J. Mod. Opt.* **57**, 756–764 (2010).
2. P. Guo and A. J. Devaney, "Comparison of reconstruction algorithms for optical diffraction tomography," *J. Opt. Soc. Am. A* **22**, 2338–2347 (2005).
3. G. Bao and P. Li, "Numerical solution of inverse scattering for near-field optics," *Opt. Lett.* **32**, 1465–1467 (2007).
4. G. Oliveri, Y. Zhong, X. Chen, and A. Massa, "Multiresolution subspace-based optimization method for inverse scattering problems," *J. Opt. Soc. Am. A* **28**, 2057–2069 (2011).
5. D. L. Marks, T. S. Ralston, S. A. Boppart, and P. S. Carney, "Inverse scattering for frequency-scanned full-field optical coherence tomography," *J. Opt. Soc. Am. A* **24**, 1034–1041 (2007).
6. E. A. Marengo, R. D. Hernandez, and H. Lev-Ari, "Intensity-only signal-subspace-based imaging," *J. Opt. Soc. Am. A* **24**, 3619–3635 (2007).
7. X. Chen, "MUSIC imaging applied to total internal reflection tomography," *J. Opt. Soc. Am. A* **25**, 357–364 (2008).
8. P. C. Chaumet, K. Belkebir, and R. Lencrherot, "Three-dimensional optical imaging in layered media," *Opt. Express* **14**, 3415–3426 (2006).
9. Q. H. Liu, Z. Q. Zhang, T. Wang, J. Bryan, G. Ybarra, L. Nolte, and W. Joines, "Active microwave imaging. I. 2-D forward and inverse scattering methods," *IEEE Trans. Microwave Theory Tech.* **50**, 123–133 (2002).
10. W. J. Walecki and F. Szondy, "Integrated quantum efficiency, reflectance, topography and stress metrology for solar cell manufacturing," *Proc. SPIE* **7064**, 70640A (2008).
11. H. Ammari, E. Iakovleva, and D. Lesselier, "A MUSIC algorithm for locating small inclusions buried in a half-space from the scattering amplitude at a fixed frequency," *Multiscale Model. Simul.* **3**, 597–628 (2005).
12. W. Zhang and A. Hoorfar, "Through-the-wall target localization with time reversal MUSIC method," *Prog. Electromagn. Res.* **106**, 75–89 (2010).
13. E. Iakovleva, S. Gdoura, and D. Lesselier, "Multistatic response matrix of a 3-D inclusion in half space and MUSIC imaging," *IEEE Trans. Antennas Propag.* **55**, 2598–2609 (2007).
14. X. Chen and Y. Zhong, "MUSIC electromagnetic imaging with enhanced resolution for small inclusions," *Inverse Probl.* **25**, 015008 (2009).
15. X. Chen, "Multiple signal classification method for detecting point-like scatterers embedded in an inhomogeneous background medium," *J. Acoust. Soc. Am.* **127**, 2392–2397 (2010).
16. X. Chen, "Signal-subspace method approach to the intensity-only electromagnetic inverse scattering problem," *J. Opt. Soc. Am. A* **25**, 2018–2024 (2008).
17. Y. Zhong and X. Chen, "MUSIC imaging and electromagnetic inverse scattering of multiple scattering small anisotropic spheres," *IEEE Trans. Antennas Propag.* **55**, 3542–3549 (2007).
18. C. Prada, S. Manneville, D. Spoliansky, and M. Fink, "Decomposition of the time reversal operator: detection and selective focusing on two scatterers," *J. Acoust. Soc. Am.* **99**, 2067–2076 (1996).
19. A. Dubois, K. Belkebir, and M. Saillard, "Localization and characterization of twodimensional targets buried in a cluttered environment," *Inverse Probl.* **20**, S63–S79 (2004).
20. A. Devaney, "Time reversal imaging of obscured targets from multistatic data," *IEEE Trans. Antennas Propag.* **53**, 1600–1610 (2005).
21. L. W. Li, P. S. Kooi, M. S. Leong, and T. S. Yeo, "On the eigenfunction expansion of dyadic Green's function in planarly stratified media," *J. Electromagn. Waves Appl.* **8**, 663–678 (1994).
22. X. Chen, Y. Zhong, and K. Agarwal, "Subspace methods for solving electromagnetic inverse scattering problems," *Methods Appl. Anal.* **17**, 407–432 (2010).